Journal of Multidisciplinary Engineering Science Studies (JMESS)
ISSN: 2458-925X
Vol. 9 Issue 4, April - 2023

Physically Activated Nut Residues As Strontium And Manganese Adsorbents From Contaminated Waters - Equilibrium And Isotherm Models

Despina Vamvuka*, Despina Pentari, Vasiliki Stathopoulou, Elena Sdokou
School of Mineral Resources Engineering, Technical University of Crete, Chania, Greece
*corresponding author email: vamvuka@mred.tuc.gr

***Abstract*— Two nut residues were investigated for their potential to adsorb strontium and manganese from wastewaters. Raw materials were physically activated by nitrogen and steam at 700°C in a fixed bed system. Biochars were characterized in terms of proximate and elemental analyses, specific surface area and pore volume, mineral phases and chemical functional groups. Kinetic and adsorption experiments were conducted at actual pH and a series of initial ion concentrations. Equilibrium and adsorption data were modelled by applying pseudo-first/second order models and Langmuir/Freundlich isotherm models, respectively. Both biochars presented negatively charged functional groups on their surface, were enriched in alkaline minerals and attained high specific surface areas. Intense adsorption of Sr and Mn ions took place within 15 min contact time. Removal efficiency of Sr and Mn from the solution by almond kernel biochar reached maximum values of 99.1% and 97.8%, respectively, whereas by walnut kernel biochar 85.1% and 99.6%, respectively. Experimental data of both biochars were better fitted by the Langmuir model, with maximum adsorption capacity of 12.3 mg/g Sr and 13.4 mg/g Mn for almond kernel and 8.7 mg/g Sr and 23.4 mg/g Mn for walnut kernel.**

Keywords—biochar; Sr adsorption; Mn adsorption

I. INTRODUCTION

Strontium is one of the main components of radioactive waste effluents produced from reprocessing of nuclear fuels. Also, it is discharged from ceramic and fire cracker industries, from coal mines, as well as municipal solid waste management and agricultural processing industries. Its long life, high solubility in aqueous solutions and bioaccumulation in food chains or drinking water, makes strontium fatal for living beings. On the other hand, manganese is found in earth's crust and groundwater and is an essential micronutrient for plants, animals and humans through biological processes [1]. However, excessive amounts of manganese in wastewaters from various industries including coal mining, metal plating and textiles, become toxic for organisms, causing serious health problems [2-4].

Various techniques have been proposed for the removal of strontium or manganese from polluted aqueous media, such as solvent extraction, electro-coagulation, evaporation, ion-exchange, membrane separation and adsorption. Among these techniques, the latter is gaining increased attention, because of its simplicity, flexibility, efficiency, economic feasibility and absence of toxic by-products [2,4-6].

A wide range of adsorption materials have been used including clays, silica gel, zeolites, synthetic polymers, active carbons and carbon nanotube/iron oxide magnetic composites [5-9]. However, the high cost, the complexity of preparation and recovery and the potential risk of secondary pollution limit the applicability of these adsorbents.

Recently, a promising, inexpensive, environmentally green adsorbent is perceived to be biochar, a carbon-rich material produced from thermal decomposition of lignocellulosic, animal, or other organic wastes. The removal efficiency of heavy metals from aqueous solutions is dependent on the physical and chemical properties of biochar, especially the internal structure and surface functional groups, which in turn are influenced not only by feedstock type, but also by the operating conditions during thermal treatment [1,2,5,6]. Removal of strontium by wood, chicken manure and food waste biochars was reported to be 19.4-26.7 mg/g [10] and by sawdust 0.74 mg/g [11], while the maximum adsorption capacity of bone char, manure-derived biochars, sewage sludge, rice husk and date palm biochars for manganese, ranged between 2.4 mg/g and 6.6 mg/g [1,2,12,13]. This low efficiency for practical applications, has led researchers to develop various modification methods in order to improve the adsorption properties of biochars. Alkali-treated biochars of residual coffee, peanut husk, sugarcane bagasse and wood/food waste achieved adsorption capacities for strontium between 5.5 mg/g and 43 mg/g [10,14,15]. Almond green hull, chemically treated with H_2O_2 and HNO_3, reached a value of 116 mg/g [16]. On the other hand, a NaOH-modified biochar derived from pomelo peel showed an

adsorption capacity for manganese up to 163 mg/g [6], whereas acrylonitrile grafted cellulose functionalized with hydrazine hydrate showed a capacity of only 5.8 mg/g [4].

Given the limited research on the valorization of nut residues from corresponding food industries and the lack of a comparative study for strontium and manganese removal from contaminated waters by biochar materials, present work aimed to investigate the potential of such residues as efficient adsorbents of strontium and manganese, without using any chemicals, but an environmentally friendly activation method instead. Thus, raw materials were physically activated by nitrogen and steam and biochars were characterized by chemical, structural and mineralogical analyses. Adsorption experiments were conducted for a series of Sr and Mn ion concentrations and adsorption data were modeled by Langmuir/Freundlich isotherm models.

II. MATERIALS AND METHODS

A. Materials Preparation

The raw materials used in present work were almond and walnut kernels, provided by private nut industries in North Greece. These were riffled and ground in a cutting mill to a particle size below 500 μm and devolatilized in a fixed bed system at 700°C. The stainless steel reactor was charged with about 15 g of sample, placed onto a grid basket supported by a rod, tightly capped and inserted into the furnace. After flushing with nitrogen of flow rate 200 mL/min for 30 min, the furnace was set to the final temperature at a heating rate of 10 °C/min and sustained at this temperature for 30 min. Volatile products were collected in salt-ice baths. After cooling under nitrogen, the biochar was weighed and a mass balance was performed.

After pyrolysis, each biochar was again loaded into the reactor and heated in nitrogen up to 700°C. Nitrogen was then switched to steam, by injecting distilled water with a flow rate of 0.5 mL/min, through an automatic syringe pump. A 2 m pipe surrounding the reactor enabled a uniform steam flow over the char bed. Activation by steam lasted 1 h, after which the system was cooled under nitrogen.

B. Materials Characterization

Raw materials and biochars were characterized by proximate and ultimate analysis, according to the CEN/TC335 European standards. Programmable laboratory furnaces and a Flash 2000 CHNS Thermo-Scientific analyzer were used. Specific surface area, micropore volume and pore size were determined by the BET method. Prior to each test, the samples were out-gassed overnight at 150°C under vacuum. Liquid nitrogen adsorption data were obtained at relative pressures of 0.03-0.35, using an automatic volumetric apparatus, model Nova 2200 of Quantachrome.

Mineral phases were detected by an X-ray diffractometer (XRD), model S2 Ranger/EPS of Bruker AXS, at scanning range from 2 to 70 2θ°, with increments of 0.02°/s and identified using DIFFRAC plus Evaluation software and JCPDS database.

Chemical functional groups were detected by an FTIR spectrophotometer, model Spectrum 100 of Perkin Elmer. FTIR spectra of pellets, consisting of sample/KBr at a ratio of 1/100 w/w, were recorded in the range of 400-4000 cm^{-1} wave number, at a resolution of 4 cm^{-1}.

C. Adsorption Experiments

$Sr(NO_3)_2$ and $MnSO_4.H_2O$ of analytical grade, purchased by Sigma-Aldrich Chemical Co, were used to prepare stock solutions of 1000 mg/L Sr/Mn in de-ionized water. Standard solutions with ion concentration of 1, 5, 10, 25, 50, 75, 100 mg/L were then obtained by dilution.

In order to investigate the kinetics of adsorption, each biochar with a dose of 4 g/L was mixed with a 10 mg/L metal-containing standard solution and agitated on a mechanical shaker at 200 rpm at room temperature, for specific contact time intervals of 15, 30, 60, 120, 180 and 300 min. Liquid suspensions were withdrawn at the end of each time interval and filtered through microporous Whatman filters. The tests were conducted at actual pH without any adjustment, which was measured by a bench Metter Toledo pH-meter, before and after metal adsorption. The concentration of metals in the filtrates was measured by an inductively coupled plasma mass spectrometer, model ICP-MS 7500cx of Agilent Technologies, assisted by an Anton Paar Multiwave 3000 oven for samples digestion.

Following the kinetic experiments, the retention of metals by the biochars was investigated by carrying out adsorption tests, until equilibrium was reached, for the range of ion concentrations mentioned above, at the same experimental conditions. Duplicate tests were performed and the average values are reported below.

D. Modeling of Equilibrium and Adsorption Data

The interpretation of experimental equilibrium data was performed by applying the pseudo-first order model of Lagergreen (eq. 1) and the pseudo-second order model (eq. 2) [17]:

$$\log(q_e - q_t) = \log q_e - \frac{k_1}{2.303} t \quad (1)$$

$$\frac{t}{q_t} = \frac{1}{k_2 q_e^{\,2}} + \frac{t}{q_e} \quad (2)$$

where, q_t and q_e (mg/g) are the amount of metal sorbed at time t and at equilibrium time, respectively, and k_1, k_2 (1/h) are the rate constants for the pseudo-first order and pseudo-second order kinetics. k_1 and q_e values of eq. (1) were obtained from the linear plot of log (q_e-q_t) versus t, whereas k_2 and q_e values from eq. (2) were obtained from the plot of t/q_t versus t.

In order to characterize the sorption process and evaluate the adsorption capacity of the biochars

studied for Sr and Mn ions, the Langmuir (eq. 3) and Freundlich (eq. 4) isotherm models were adopted [17]:

$$\frac{C_e}{q_e} = \frac{1}{bC_e} + \frac{C_e}{Q} \quad (3)$$

$$\log q_e = \log k + \frac{1}{n}\log C_e \quad (4)$$

where, C_e is the equilibrium ion concentration in the solution (mg/L), q_e is the amount of ion adsorbed per adsorbent mass unit (mg/g) at equilibrium, b is a parameter indicating the adsorption energy (L/mg), Q is a parameter expressing the maximum metal uptake (mg/g), k is the Freundlich distribution coefficient indicating adsorption capacity (L/g) and 1/n is a dimensionless parameter indicating adsorption intensity. For the Langmuir model the separation factor R_L was calculated, in order to predict whether adsorption was "favourable" or "unfavourable" as follows:

$$R_L = \frac{1}{1+bC_e} \quad (5)$$

For R_L>1 adsorption was unfavourable, for R_L=1 linear, for 0<R_L<1 favourable and for R_L=0 irreversible. Isotherm constants were determined using a non-linear solver.

The adsorption efficiency was calculated as follows:

$$\%Meremoval = \frac{C_0 - C_e}{C_0} x100 \quad (6)$$

The amount of metal adsorbed per adsorbent mass unit (uptake) q (mg/g) was calculated by:

$$q = \frac{(C_0 - C)V}{m} \quad (7)$$

where C_0 and C are the initial and final metal concentrations (mg/L) in the solution, V is the solution volume (L) and m is the mass of adsorbent used (g).

III. Results and Discussion

A. Physical and Chemical Characteristics of Raw Materials and Biochars

The proximate and ultimate analysis of raw almond and walnut residues and their biochars is indicated in Table I. Both samples were rich in volatile matter, while they were free of sulphur and had low ash and nitrogen contents. Thermal decomposition at 700°C resulted in a significant reduction of hydrogen and oxygen, due to dehydration-decarboxylation reactions [18], leaving a solid material enriched in carbon and with higher stability [18,19].

The yield of biochars after pyrolysis under an atmosphere of nitrogen and after activation by steam at 700°C is compared in Figure 1. As can be observed, a lower amount of biochars was produced upon steam gasification, as the chars were principally converted to CO, H_2 and CO_2 gases through equations (8) and (9) below:

$$C + H_2O \rightarrow CO + H_2 \quad (8)$$

$$CO + H_2O \rightarrow CO_2 + H_2 \quad (9)$$

The specific surface area, pore volume and size are important factors for the adsorption capacity of biochars. The structural characteristics of the nut residues biochars generated after pyrolysis in nitrogen, or combined pyrolysis-steam activation, are included in Table II. As clearly shown, microporosity

TABLE I. Proximate and Ultimate Analysis of Raw Materials and Biochars

Sample	Volatile Matter	Fixed Carbon	Ash	C	H	N	O	S
Almond kernel (AK)								
raw	72.8	26.7	0.5	54.0	6.1	0.3	39.1	-
biochar	-	98.8	1.2	83.6	1.5	0.9	12.8	-
Walnut kernel (WK)								
raw	76.5	20.6	2.9	47.5	6.0	0.9	42.7	-
biochar	-	90.0	10.0	83.3	1.5	0.8	4.4	-

TABLE II. Structural Characteristics of Biochars

Sample	Activation Gas	Specific Surface Area (m^2/g)	Micropore Volumex10^2 (cm^3/g)	Average Pore Size (Å)
AK	N_2	171.5	11.6	26.8
	N_2-H_2O_v	655.7	33.2	24.5
WK	N_2	279.0	16.4	23.3
	N_2-H_2O_v	649.1	40.4	30.0

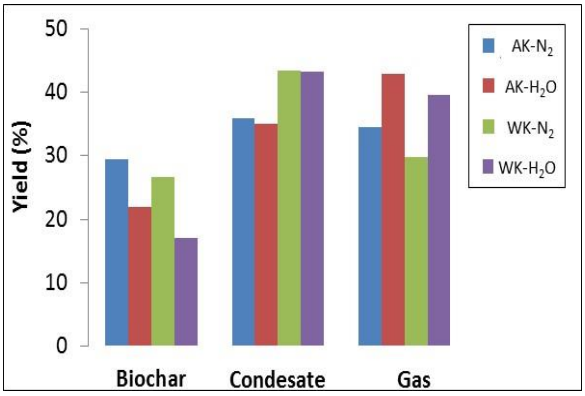

Fig. 1. *Yield of biochars after activation by N_2 or H_2O_v*

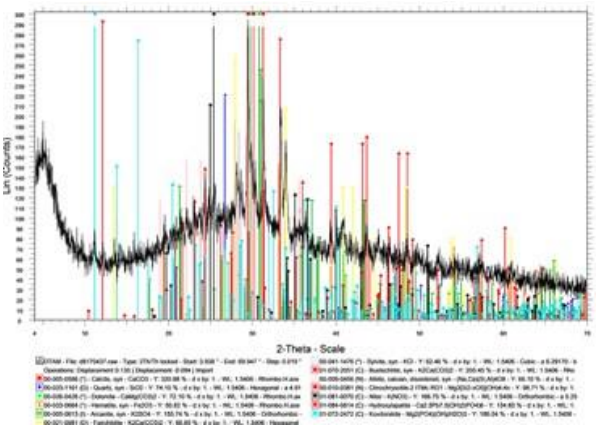

(a)

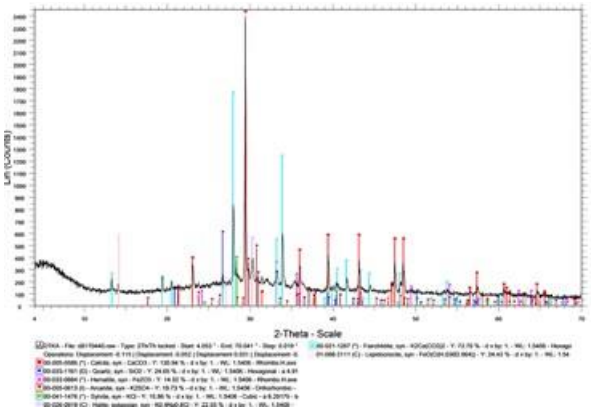

(b)

Fig. 2. *XRD spectra of (a) almond kernel and (b) walnut kernel biochars*

and specific surface area were greatly enhanced after treatment with steam by 2.3-3.8 fold. Almond kernel reached a value of 655.7 m^2/g, whereas walnut kernel a value of 649.1 m^2/g. The increase in surface area of chars by steam gasification is in agreement with previous investigations [20,21], reporting values between 601 m^2/g and 792 m^2/g for similar materials, at higher temperatures, 850-900°C.

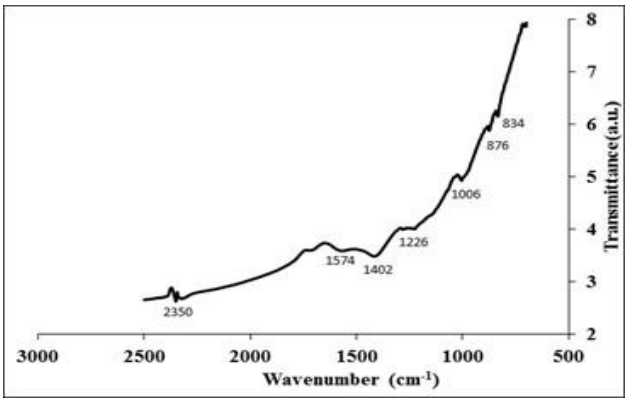

(a)

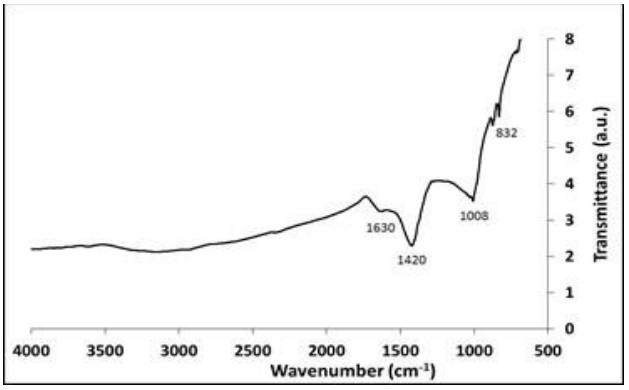

(b)

Fig. 3. FTIR spectra of *(a) almond kernel and (b) walnut kernel steam activated biochars*

B. Mineral Phases and Chemical Functional Groups of Biochars

The XRD spectra of almond kernel and walnut kernel biochars are illustrated in Figure 2. Both samples were rich in Ca and K phases, mainly present in the forms of calcite, dolomite, fairchildite, buetschliite and arcanite, sylvite, respectively. Almond kernel contained a considerable amount of P, incorporated in hydroxylapatite and kovdorskite. Si was bound in quartz, albite and clinochrysotile, whereas Fe was found in small amounts in hematite and lepidocrocite. In general, both biochars were enriched in alkali and alkaline earth minerals. Previous studies [6,10] have shown that these minerals act as adsorption sites for elements such as Sr and Mn, facilitating their removal from contaminated water.

The FTIR spectra of the two biochars obtained after steam activation are represented in Figure 3. The peaks in the range 830-880 cm^{-1} are attributed to C-H bending vibration, for aromatic out of plane deformation. The peak at 876 cm^{-1} indicates the presence of carbonates CO_3^{-2} [5]. At 1006 cm^{-1} and 1008 cm^{-1} almond and walnut kernels presented C=C alkene groups, whereas the peak of almond kernel at 1226 cm^{-1} is associated with C-O stretching vibration from alcohols and ethers. At wave numbers 1402 cm^{-1} and 1420 cm^{-1}, the biochars show the C-O

asymmetric stretching vibration in $–COO^-$ and CO_3^{-2} functional groups, or O-H stretching of alcohols. The bands at 1574 cm^{-1} and 1630 cm^{-1} can be assigned to C=C stretching of cycloalkenes. Finally, the peak of almond kernel at 2350 cm^{-1} indicates a vibrational stretching of O=C=O. The presence of negatively charged functional groups, such as carbonate, carboxyl, carbonyl and hydroxyl, located at biochar surface, plays an important role as active sorption sites, for positively charged metal ions during the adsorption process [5,14]. The FTIR analysis results are in agreement with those observed for various biochar materials [11,13,14,22].

C. Adsorption Kinetics

The effect of contact time on the sorption of Sr and Mn ions, by almond and walnut kernel biochars, is illustrated in Figures 4 and 5, respectively. As clearly shown, the adsorption rate was very rapid within the first 15 min for both biochars and metals studied. At this contact time almond kernel biochar removed 92.2% of Sr and 95.7% of Mn from the aqueous solution, while walnut kernel biochar eliminated 75.8% of Sr and 96.6% of Mn from the solution. In the case of almond kernel biochar, equilibrium was achieved in 3 h for Sr adsorption and in 2 h for Mn adsorption. The corresponding contact times for equilibrium, for walnut kernel biochar, were 1 h for Sr and 3 h for Mn sorption. The intense adsorption of these ions during the initial stages of the process was also observed in previous studies [2,6,11,14,23] and could be assigned to the high efficiency and readily available sites on the adsorbent surface. A fast initial sorbent rate is beneficial for wastewater treatment plants, by increasing the process efficiency, while minimizing the operational cost [2]. Contact times for equilibrium to be reached have been reported between 1 h and 6 h for Sr [5,11,14,15] and 1 h and 24 h for Mn [1,2,6,23], for agricultural biochar materials. Such variations in contact times reveal the strong dependence of sorption kinetics on the physical and chemical characteristics of the biochars.

The results of the pseudo-first and pseudo-second order models applied to describe the kinetics of Sr and Mn adsorption onto the biochars are included in Tables III and IV, respectively. As clearly shown, the pseudo-second order model fitted the experimental results with high accuracy, for both almond and walnut kernel biochars. This implies that the rate limiting step was chemisorption between adsorbent and adsorbate.

D. Adsorption Capacity of Biochars and Isotherm Modelling

Strontium adsorption

The adsorption capacity of biochars, as a function of the initial Sr concentration in the aqueous solution, is represented in Table V. Removal efficiency was quite high and increased with initial Sr concentration, reaching a maximum at 10 ppm Sr of 99.1% for almond kernel biochar and 85.1% for walnut kernel biochar. At higher initial concentrations uptake of

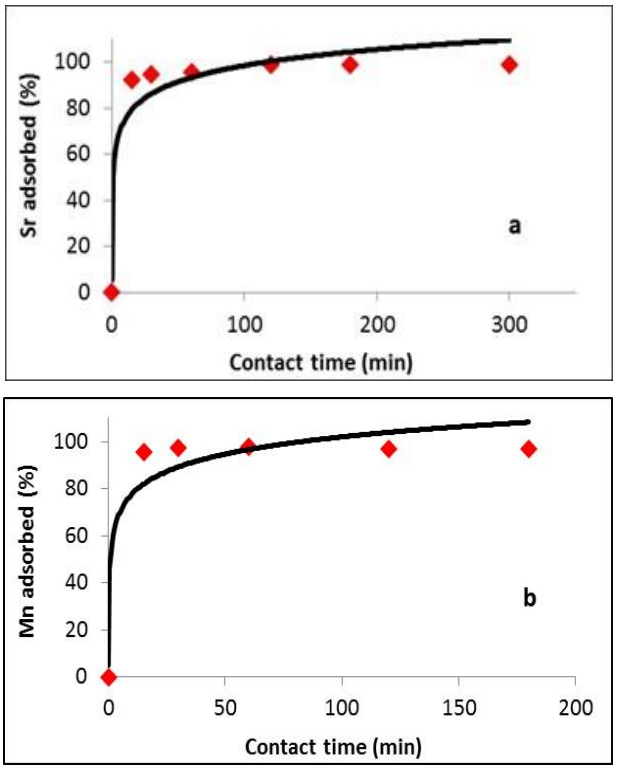

Fig. 4. Effect of contact time on sorption of (a) Sr and (b) Mn by almond kernel biochar

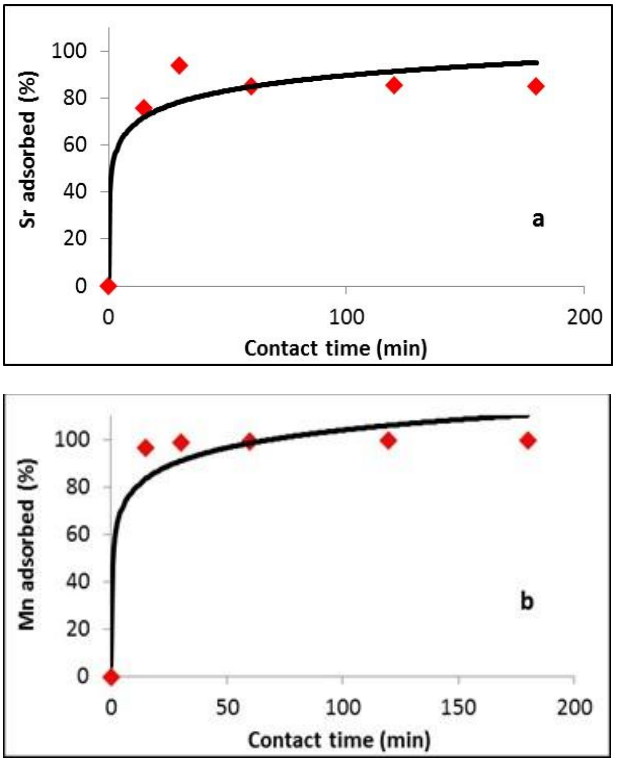

Fig. 5. Effect of contact time on sorption of (a) Sr and (b) Mn by walnut kernel biochar

TABLE III. KINETIC AND ISOTHERM MODEL PARAMETERS FOR STRONTIUM ADSORPTION

	Kinetic model parameters					
	Pseudo-first order			***Pseudo-second order***		
	q_e (mg/g)	k_1 (1/h)	R^2	q_e (mg/g)	k_2 (1/h)	R^2
Sample						
AK	2.479	0.016	0.459	2.479	0.401	1
WK	2.351	0.017	0.078	2.351	0.468	0.998
	Isotherm model parameters					
	Langmuir			***Freundlich***		
	Q (mg/g)	b (L/mg)	R^2	k (L/g)	1/n	R^2
AK	11.820	0.258	0.945	2.513	0.403	0.893
WK	10.204	0.050	0.835	0.160	0.670	0.822

TABLE IV. KINETIC AND ISOTHERM MODEL PARAMETERS FOR MANGANESE ADSORPTION

	Kinetic model parameters					
	Pseudo-first order			***Pseudo-second order***		
	q_e (mg/g)	k_1 (1/h)	R^2	q_e (mg/g)	k_2 (1/h)	R^2
Sample						
AK	2.446	0.004	0.023	2.446	0.413	1
WK	2.493	0.016	0.459	2.493	0.401	1
	Isotherm model parameters					
	Langmuir			***Freundlich***		
	Q (mg/g)	b (L/mg)	R^2	k (L/g)	1/n	R^2
AK	14.306	0.396	0.977	2.913	0.604	0.704
WK	25.641	1.262	0.969	10.449	0.619	0.948

metal decreased, due to the progressive saturation of adsorbent active sites. The pH of each solution after Sr adsorption is also shown in Table V, because this parameter is important in governing the physical and chemical behaviour of the ion in the solution. The pH before the adsorption of metal was alkaline (10.2 for almond kernel and 10.4 for walnut kernel), due to the enrichment of biochars in alkaline minerals, as previously discussed. Table V indicates that there was a small drop in pH after Sr adsorption, so that the surface remained negatively charged favoring electrostatic attraction of Sr, or formation of surface complexes [5,17]. Similar results have been found by other researchers [5,14,15].

Surface complexation, ion exchange and coordination of d-electrons of metal with aromatic π electrons adsorbent, are some of the complex mechanisms responsible for Sr sorption [10,17]. As shown above, both biochars studied had similar surface area and alkaline minerals, which could be dissolved in water increasing ion exchange at the surface sites. Hence, the better performance of almond kernel biochar towards removal of Sr from the solution could be attributed to its enrichment in negatively charged oxygen functional groups, which could facilitate complexation of Sr at the biochar surface.

The mechanism of adsorption of Sr ions on biochar surface was further investigated by employing the Langmuir and Freundlich isotherm models. Table III and Figure 6 illustrate that experimental data were better fitted by the Langmuir model, suggesting the formation of a monolayer of the adsorbate at the

TABLE V. ADSORPTION CAPACITY OF BIOCHARS FOR STRONTIUM

Initial Sr concentration (mg/L)	**Removal efficiency (%)**		**pH after adsorption**	
	AK	***WK***	***AK***	***WK***
1	98.9	54.3	9.8	9.9
5	93.2	70.2	9.6	9.8
10	99.1	85.1	9.5	9.8
25	68.8	47.2	9.3	9.7
50	58.5	37.4	9.1	9.6
75	57.2	38.0	8.9	9.3
100	49.0	34.7	8.6	9.0

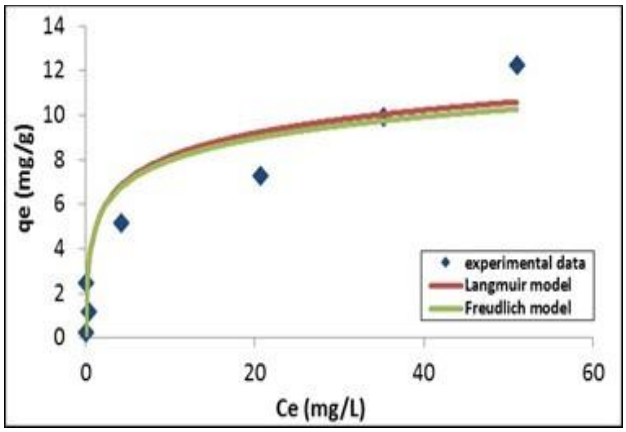

(a)

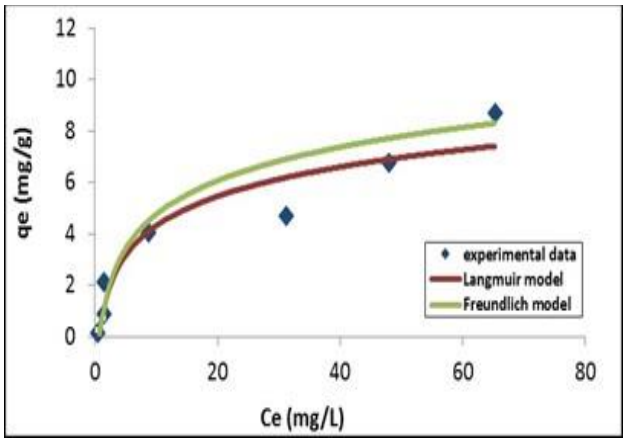

(b)

Fig. 6. Isotherm models for Sr adsorption by (a) almond kernel and (b) walnut kernel biochars

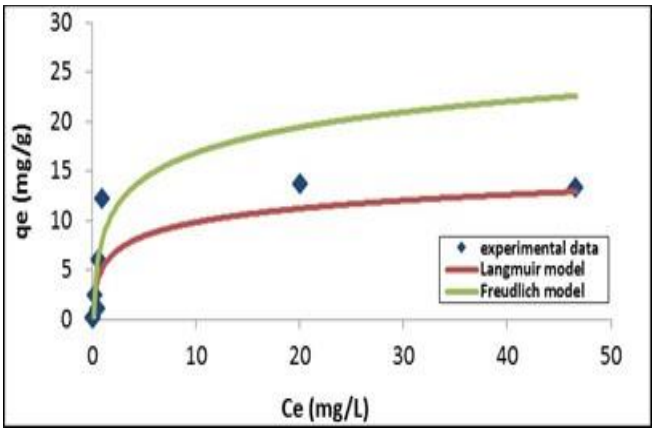

(a)

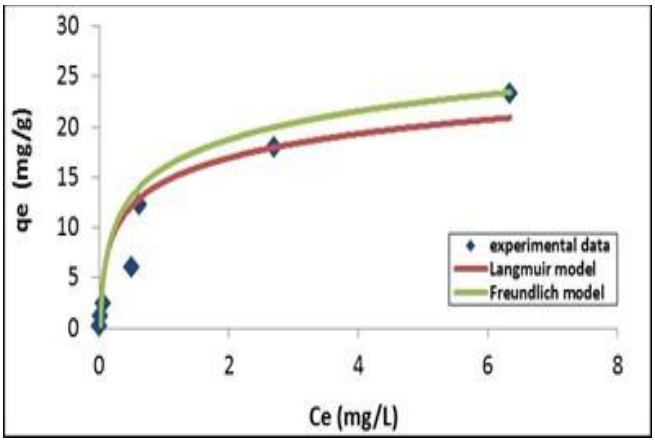

(b)

Fig. 7. Isotherm models for Mn adsorption by (a) almond kernel and (b) walnut kernel biochars

homogeneous surface of the biochars. The R_L value of the model, lying between 0 and 1, revealed a favorable adsorption process. The maximum adsorption capacity of almond kernel was 12.3 mg/g and that of walnut kernel 8.7 mg/g, values comparable to those obtained from other unmodified biochar materials [10,11].

Manganese adsorption

Table VI presents the percentage of Mn removal from the aqueous solution, in relation to the initial concentration of the metal. Adsorption efficiency was high for almost all Mn concentrations studied, achieving maximum values 97.8% for almond kernel and 99.6% for walnut kernel at 10 ppm Mn. Adsorption capacity increased with initial Mn concentration, implying that a higher amount of metal could provide more adsorbate ions to the biochars. However, at an initial concentration of 100 ppm, saturation of almond kernel surface was obvious, while uptake of Mn by walnut kernel biochar was still high. As in the case of Sr, the alkaline pH of the solution after adsorption acquired more negative charges to the adsorbent surface, favoring electrostatic attraction with Mn cations, or complexation with negatively charged functional groups, which is in agreement with previous studies [1,2,4,6,8,13,23]. The reduction of pH observed in Table VI, at initial concentrations above 10 ppm, suggests that precipitation of manganese carbonate or manganite, as reported by some investigators [23], was unlike.

TABLE VI. ADSORPTION CAPACITY OF BIOCHARS FOR MANGANESE

Initial Mn concentration (mg/L)	Removal efficiency (%)		pH after adsorption	
	AK	*WK*	*AK*	*WK*
1	97.5	99.4	10.5	9.8
5	90.9	99.6	10.4	9.8
10	97.8	99.4	10.0	9.7
25	97.7	99.0	9.6	9.1
50	97.5	98.8	8.9	8.1
75	80.1	96.5	8.6	7.9
100	53.4	93.7	8.2	7.8

Possible mechanisms explaining the adsorption capacity of biomass towards Mn ion, as also stated above, are functional group complexation, cation exchange and coordination of metal ions with adsorbent electrons [13,17]. Walnut kernel biochar presented a better performance in this case. The relationship between sorption capacity and equilibrium concentrations was described by applying the Langmuir and Freundlich isotherm models, as before. Related parameters are included in Table IV and fitting curves are shown in Figure 7. The results indicate that Langmuir model was the adequate model fitting to the experimental data, indicating that there was a homogeneous monolayer on adsorbent surface, where adsorption took place. The R_L parameter, calculated between 0 and 1, implied a favorable process. Almond kernel biochar possessed a maximum adsorption capacity of 13.4 mg/g, whereas walnut kernel a maximum adsorption capacity of 23.4 mg/g. Literature data values ranged between 2.4 mg/g and 6.6 mg/g, for different unmodified sorbent materials [1,2].

IV. CONCLUSIONS

Almond and walnut kernel biochars studied, after physical activation by steam at 700°C presented negatively charged functional groups on their surface, were enriched in alkali and alkaline earth minerals and attained a specific surface area of 655.7 m^2/g and 649 m^2/g, respectively. Intense adsorption of Sr and Mn ions took place within 15 min contact time, while equilibrium was achieved in 1-3 h for Sr adsorption and 2-3 h for Mn adsorption. The pseudo-second order model fitted adsorption kinetics with high accuracy.

Removal efficiency of Sr and Mn from the solution, at actual unadjusted pH, by almond kernel biochar reached maximum values of 99.1% and 97.8%, respectively, whereas by walnut kernel biochar 85.1% and 99.6%, respectively. Experimental data of both biochars were better fitted by the Langmuir model, with maximum adsorption capacity of 12.3 mg/g Sr and 13.4 mg/g Mn for almond kernel and 8.7 mg/g Sr and 23.4 mg/g Mn for walnut kernel. Possible mechanisms of Sr and Mn ions sorption include cation exchange, surface complexation and coordination of metal ions with adsorbent electrons. Almond and walnut kernel residues could be used as low cost, effective and environmentally friendly adsorbents of Sr and Mn from polluted wastewaters.

ACKNOWLEDGMENT

The authors kindly thank the laboratories of Applied Mineralogy, PVT and Core Analysis, Hydrogeochemical Engineering and Soil Remediation and Management of Mining/Metallurgical Wastes, of the Technical University of Crete, for the XRD, FTIR and ICP-MS measurements.

REFERENCES

[1] Y.H. Fseha, B. Sizirici and I. Yildiz, “Manganese and nitrate removal from groundwater using date palm biochar: Application for drinking water”, Environ. Adv., vol. 8, pp. 100237, 2022.

[2] M. Idrees, S. Batool, H. Ullah, Q. Hussain, M.I. Al-Wabel, M. Ahmad et al., “Adsorption and thermodynamic mechanisms of manganese removal from aqueous media by biowaste-derived biochars”, J. Molec. Liq., vol. 266, pp. 373-380, 2018.

[3] J. Briffa, E. Sinagra and R. Blundeil, “Heavy metal pollution in the environment and their toxicological effects on humans”, Heliyon, vol. 6, pp. e04691, 2020.

[4] F.I. Abouzayed, N.T.A. El-nasser and S.A. Abouel-Enein, “Synthesis, characterization of functionalized grafted cellulose and its environmental application in uptake of copper (II), manganese (II) and iron (III) ions”, J. Molec. Struc., vol. 1270, pp. 133907, 2022.

[5] J. Jang, W. Miran, S.D. Divine, M. Nawaz, A. Shahzad, S.H. Woo and D.S. Lee, “Rice straw-based biochar beads for the removal of radioactive strontium from aqueous solution”, Sci. Tot. Environ., vol. 615, pp. 698-707, 2018.

[6] Q. An, Y. Miao, B. Zhao, Z. Li and S. Zhu, “An alkali modified biochar for enhancing Mn adsorption: Performance and chemical mechanism”, Mater. Chem. Phys., vol. 248, pp. 122895, 2020.

[7] A.E. Burakov, E.V. Galunin, I.V. Burakova, A.E. Kucherova, S. Agarwal, A.G. Tkachev and V.K.

Gupta, “Adsorption of heavy metals on conventional and nanostructured materials for wastewater treatment purposes: a review”, Ecotoxicol. Environ. Saf., vol. 148, pp. 702-712, 2018.

[8] G. Li, H. Hao, Y. Zhuang, Z. Wang and B. Shi, “Powered activated carbon enhanced manganese (II) removal by chlorine oxidation”, Water Res., vol. 156, pp. 287-296, 2019.

[9] D. Sofronov, M. Rucki, V. Varchenko, E. Bryleva, P. Mateychenko and A. Lebedynskiy, “Removal of europium, cobalt and strontium from water solutions using MnO(OH)-modified diatomite”, J. Environ. Chem. Eng., vol. 10, pp. 106944, 2022.

[10] K.N. Palansooriya, I. Yoon, S. Kim, C. Wang, H. Kwon, S. Lee et al., “Designer biochar with enhanced functionality for efficient removal of radioactive cesium and strontium from water”, Environ. Res., vol. 214, pp. 114072, 2022.

[11] V. Chakraborty, P. Das and P.K. Roy, “Carbonaceous materials synthesized from thermally treated waste materials and its application for the treatment od strontium metal solution: Batch and optimization using Response Surface Methodology”, Environ. Technol. Innov., vol. 15, pp. 100394, 2019.

[12] J.G. Han, D.W. Fan, X.Z. Li, Y.I. Zhu and A. Sajjad, “Mechanism of Cr^{6+}, Mn^{2+}, Cu^{2+} and Cd^{2+} adsorption by a low-cost rice husk-derived biochar in aqueous solutions”, Fresen. Environ. Bull., vol. 25, pp. 2736-2744, 2016.

[13] K. Michael, A.W. Wilson and P.P. Govender, “Modelling of manganese-contaminated groundwater through batch experiments: Implications for bone char remediation”, Environ. Adv., vol. 10, pp. 100323, 2022.

[14] A. Kausar, G. MacKinnon, A. Alharthi, J. Hargreaves, H.N. Bhatti and M. Iqbal, “A green approach for the removal of Sr (II) from aqueous media: kinetics, isotherms and thermodynamic studies”, J. Molec. Liq., vol. 257, pp. 164-172, 2018.

[15] J. Shin, M. Choi, C.Y. Go, S. Bae, K.C. Kim and K. Chon, “NaOH-assisted H_2O_2 post-modification as a novel approach to enhance adsorption capacity of residual coffee waste biochars toward radioactive strontium: Experimental and theoretical studies”, J. Hazard. Mater., vol. 435, pp. 129081, 2022.

[16] A. Ahmadpour, M. Zabihi, M. Tahmasbi and T.R. Bastami, “Effect of adsorbents and chemical treatments on the removal of strontium from aqueous solutions”, J. Hazard. Mater., vol. 182, pp. 552-556, 2010.

[17] D. Vamvuka, S. Dermitzakis, D. Pentari and S. Sfakiotakis, “Valorization of meat and bone meal through pyrolysis for soil amendment or lead adsorption from wastewaters”, Food Bioprod. Process., vol. 109, pp. 148-157, 2018.

[18] D. Vamvuka, S. Sfakiotakis and O. Pantelaki, “Evaluation of gaseous and solid products from the pyrolysis of waste biomass blends for energetic and environmental applications”, Fuel, vol. 236, pp. 574-582, 2019.

[19] H. Zhang, C. Chen, E.M. Gray and S.E. Boyd, “Effect of feedstock and pyrolysis temperature on properties of biochar governing end use efficacy”, Biomass Bioenergy, vol. 105, pp. 136-146, 2017.

[20] M. Macias-Perez, A. Bueno-Lopez, M. Lillo-Rodenas, C. Salinas-Martinez de Lecea and A. Linares-Solano, “SO_2 retention on CaO/activated carbon sorbents. Part II: effect of activated carbon support”, Fuel, vol. 87, pp. 2544-2550, 2008.

[21] J. Gonzalez, S. Roman, J. Encinar and G. Martinez, “Pyrolysis of various biomass residues and char utilization for the production of activated carbons”, J. Anal. Appl. Pyrol., vol. 85, pp. 134-141, 2009.

[22] M. Xu, Y. Wu, D. Nan, Q. Lu and Y. Yang, “Effects of gaseous agents on the evolution of char physical and chemical structures during biomass gasification”, Biores. Technol., vol. 292, pp. 121994, 2019.

[23] H. Yankovych, V. Novoseltseva, O. Kovalenko, D.M. Behunova, M. Kanuchova, M. Vaclavikova and I. Melnyk, “New perception of Zn (II) and Mn (II) removal mechanism on sustainable sunflower biochar from alkaline batteries contaminated water”, J. Environ. Manag., vol. 292, pp. 112757, 2021.